Journal of Physics D: Applied Physics

PAPER

Simultaneous quantification of aqueous peroxide, nitrate, and nitrite during the plasma–liquid interactions by derivative absorption spectrophotometry

To cite this article: Bangbang He *et al* 2017 *J. Phys. D: Appl. Phys.* **50** 445207

IOP Publishing Journal of Physics D: Applied Physics
J. Phys. D: Appl. Phys. **50** (2017) 445207 (9pp) https://doi.org/10.1088/1361-6463/aa8819

Simultaneous quantification of aqueous peroxide, nitrate, and nitrite during the plasma–liquid interactions by derivative absorption spectrophotometry

Bangbang He[1], Yupengxue Ma[1], Xinning Gong[1], Zhijun Long[1], Junshuai Li[2], Qing Xiong[3], Hai Liu[1], Qiang Chen[1], Xianhui Zhang[1], Size Yang[1] and Qing Huo Liu[4]

[1] Department of Electronic Science, Fujian Provincial Key Laboratory of Plasma and Magnetic Resonance, Institute of Electromagnetics and Acoustics, Xiamen University, Xiamen 361005, People's Republic of China
[2] School of Physical Science and Technology, Lanzhou University, Lanzhou 730000, People's Republic of China
[3] State Key Laboratory of Power Transmission Equipment & System Security and New Technology, Chongqing University, Chongqing 400044, People's Republic of China
[4] Department of Electrical and Computer Engineering, Duke University, Durham, NC 27708, United States of America

E-mail: chenqiang@xmu.edu.cn

Received 24 May 2017, revised 10 August 2017
Accepted for publication 24 August 2017
Published 13 October 2017

Abstract

A derivative absorption spectroscopic method is used *in situ* to simultaneously trace and quantify the aqueous peroxide (H_2O_2), nitrate (NO_3^-) and nitrite (NO_2^-) generated during plasma–liquid interactions. The results indicate that the time evolutions of H_2O_2, NO_3^- and NO_2^- generated from the plasma–liquid interactions strongly depend on the solution's pH value, which varies with the plasma treatment. The concentrations of aqueous H_2O_2, NO_3^- and NO_2^- increase independently from each other during the plasma treatment when the solution's pH value is higher than 3.0. However, when the solution's pH value is less than 3.0, most of the aqueous NO_2^- (~71.5%) will exist in the form of molecular nitrous acid since the pK_a of nitrous acid is 3.4, the aqueous NO_3^- is mainly formed from the reaction between H_2O_2 and NO_2^- as well as the decomposition of molecular HNO_2, which leads to a continuous increase of NO_3^- concentration and an appearance of the maximum concentrations of H_2O_2 and NO_2^- as the pH value of the solution reaches 3.0.

Keywords: derivative absorption spectrophotometry, plasma–liquid interactions, peroxide, nitrate, nitrite

(Some figures may appear in colour only in the online journal)

1. Introduction

When water or aqueous solution is in contact with an air plasma, reactive oxygen and nitrogen species (RONS) are usually produced from gaseous plasma and the plasma–liquid interactions. When these RONS transport towards the liquid phase from the gaseous plasma, they either directly become aqueous species or produce new RONS by a series of reactions in bulk liquid, as well as in the plasma–liquid interface [1]. These dissolved aqueous RONS, as well as derivative species in the plasma–liquid interface, can take part in the reactions in the liquid surface and in bulk liquid, which are

responsible for the plasma-based applications, such as water treatment [2–4] and plasma medicine [5, 6]. Therefore, the tracing and quantification of the plasma–liquid generated aqueous RONS attracts intensive attention in the study of the plasma–liquid interactions. Most of the common long-lived RONS are peroxide (H_2O_2), nitrate (NO_3^-) and nitrite (NO_2^-) in the plasma–liquid interactions, especially as the plasma is operated in open air. H_2O_2 is formed mainly by a combination of hydroxyl radicals, which are generated by plasma-induced water reactions with electrons and ions [4, 7–14] in the gaseous plasma [15] and/or in the liquid depending on the type of the plasma source. Aqueous NO_3^- and NO_2^- are produced by the dissolution of plasma-induced formation of nitrogen oxides [2, 16, 17]. The quantity of aqueous H_2O_2 is usually estimated by a colorimetric method using the absorption of H_2TiO_4 at 410 nm ($Ti^{4+} + H_2O_2 + 2H_2O \rightarrow H_2TiO_4 + 4H^+$) [18–22] or the absorption of VO_2^{3+} cation at 450 nm ($VO_3^- + 4H^+ + H_2O_2 \rightarrow VO_2^{3+} + 3H_2O$) [23–26]. Because the colorimetric method needs to take part of the sample (containing H_2O_2) to react with the regent of Ti^{4+} or VO_3^- in strong acid of H_2SO_4, it is not suitable for an *in situ* measurement of plasma-induced H_2O_2. For NO_3^- and NO_2^- measurement, many techniques have been reported, such as spectrophotometric [27], fluorescent, chemiluminescent and liquid chromatography [28, 29]. The colorimetric detection with Griess reagents [30] is the mostly used spectrophotometric method. All of these techniques require either a specific reactive reagent or specialized apparatus, thus they are also not suitable for *in situ* measurement.

In order to control the generation of aqueous RONS by tuning the discharge conditions, we need to trace and quantify the evolution of the plasma generated aqueous H_2O_2, NO_3^- and NO_2^-. Herein, we present a simple, fast *in situ* measurement technique, which is based on the derivative absorption spectrophotometry [31–33]. In principle, if we assume that the absorbance of a solution obeys Beer's law, the absorbance (A) of a multi-component solution with m components can be expressed as equation (1)

$$A_\lambda = \sum_{i=1}^{m} l\varepsilon_{i\lambda}C_i, \tag{1}$$

where A_λ, l, $\varepsilon_{i\lambda}$ and C_i are the solution absorbance at wavelength λ, the sample optical path length, the extinction coefficient at wavelength λ and the concentration for the ith component, respectively. Actually, Oh *et al* have estimated the concentrations of H_2O_2, NO_3^- and NO_2^- in plasma treated water using an automated curve-fitting routine for the UV absorption spectra [34–36]. On the other hand, it is easy to obtain the standard $\varepsilon_{i\lambda}$ by individually measuring the concentration-dependent absorbance of each pure component ($A_{i\lambda} = l\varepsilon_{i\lambda}C_i$, $A_{i\lambda}$ is the absorbance of the ith component at wavelength λ). One can achieve the C_i information by solving a series of equations, and the least number of equations is the total number of the solution's components, m. For example, if we have two components in a solution and their concentrations are C_1 and C_2. We can select two different wavelengths of λ and λ', then the absorbances of the solution at λ and λ' can be expressed as

$$A_\lambda = l\varepsilon_{1\lambda}C_1 + l\varepsilon_{2\lambda}C_2 \tag{2}$$

$$A_{\lambda'} = l\varepsilon_{1\lambda'}C_1 + l\varepsilon_{2\lambda'}C_2. \tag{3}$$

If $\varepsilon_{1\lambda}$, $\varepsilon_{2\lambda}$, $\varepsilon_{1\lambda}'$, and $\varepsilon_{2\lambda}'$ are known from the above mentioned method, C_1 and C_2 can be obtained by solving equations (2) and (3). For the solution containing m components, in principle, one can select m different wavelengths and m equations to achieve C_i. If the solution components have overlapping absorption bands or the absorption obeys a modified Beer's law, such as $A_{i\lambda} = l\varepsilon_{i\lambda}C_i + b$ (b is a constant indicating a baseline shift of the absorbance), a considerable error will be induced in the estimated C_i when using the absorbance [37]. This problem can be solved by using derivative spectra to resolve the overlapping bands and/or to remove the baseline shift effect in the quantitative analysis. That is to say, equation (1) becomes

$$\frac{\mathrm{d}^n A_\lambda}{\mathrm{d}\lambda^n} = l\sum_{i=1}^{m}\frac{\mathrm{d}^n\varepsilon_{i\lambda}}{\mathrm{d}\lambda^n}C_i, \tag{4}$$

where $\mathrm{d}^nA_\lambda/d_\lambda^n$ and $\mathrm{d}^n\varepsilon_{i\lambda}/\mathrm{d}_\lambda^n$ are the nth order of the derivatives for the solution absorbance and the extinction coefficient of the ith component at wavelength λ, respectively. Similar to the above mentioned procedure, C_i can be obtained by solving a series of equations if we have the standard $\mathrm{d}^n\varepsilon_{i\lambda}/\mathrm{d}\lambda^n$ of each component.

$l\mathrm{d}^n\varepsilon_{i\lambda}/\mathrm{d}\lambda^n$ can be obtained by linearly fitting the curve of $\mathrm{d}^nA_{i\lambda}/\mathrm{d}\lambda^n$ versus C_i based on the formula of $\mathrm{d}^nA_{i\lambda}/\mathrm{d}\lambda^n = l\mathrm{d}^n\varepsilon_{i\lambda}/\mathrm{d}\lambda^nC_i$. If there are isosbestic wavelengths for the derivative absorbance of the solution components ($\mathrm{d}^n\varepsilon_{i\lambda}/\mathrm{d}\lambda^n = 0$ at these wavelengths), the solving process of equation (4) will be more simplified when these isosbestic points are included in the m different wavelengths. Suzuki *et al* have used the isosbestic wavelengths to estimate concentrations of NO_3^-, and NO_2^- by a second derivative spectrophotometry [38]. Most importantly, the influences of interference from scattering, matrix or other absorbing compounds can also be reduced by using derivative spectrophotometry [37]. In this study, we use the first order derivative of the liquid absorbance to perform *in situ* simultaneous quantification of aqueous H_2O_2, NO_3^- and NO_2^- generated during the plasma–liquid interactions.

For practical applications, m equations for m components are usually not very effective in extracting C_i because it involves relative errors in the final results. To reduce the error in the estimation for a multi-component solution, usually the number of equations (the number of the selected wavelengths) is much larger than the least-required equation number. For the over-required equations, the estimation error can be reduced by a multivariable linear regression process [37, 39–41].

2. Experimental

The plasma is ignited on a flowing liquid surface as illustrated in figure 1, which is similar to the setup used by Jamroz *et al* [2] in a study of plasma-induced generation of active species and wastewater treatment. The cylinder-like plasma reactor is made from polytetrafluoroethylene

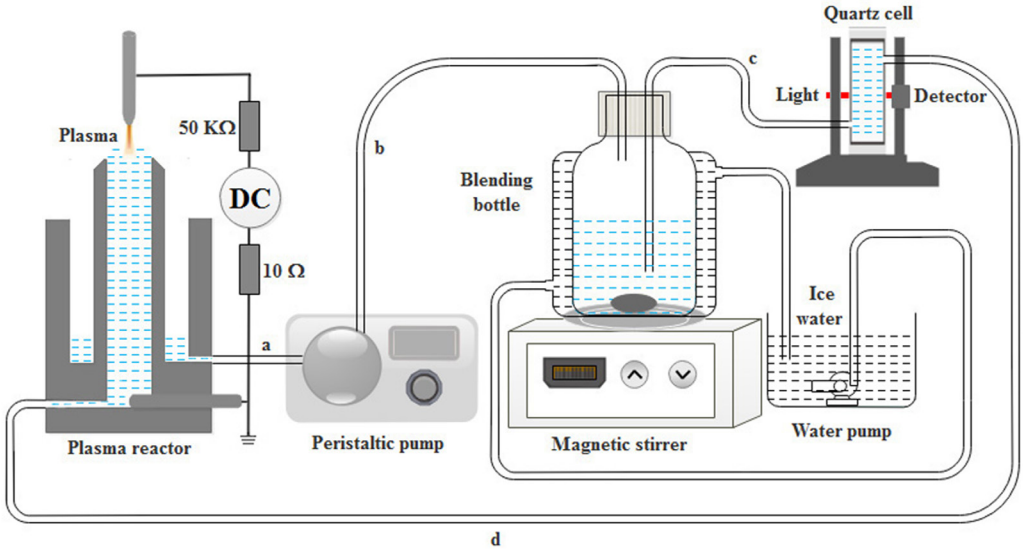

Figure 1. Schematic diagram of the experimental setup. Lengths of silicone tubes *a*, *b*, *c* and *d* are 20 cm, 20 cm, 25 cm and 25 cm, respectively. The inner and outer diameters of the tubes are 3 and 5 mm, respectively. Insider the pump, there is a 10 cm-silicone tube (4 and 6 mm in inner and outside diameters) to connect tubes *a* and *b*.

(see appendix for details of its geometric parameters). The plasma treated liquid (100 ml) is circulated by a peristaltic pump with a flow rate of 100 ml min^{-1}. The silicone tube is 3 mm in inner diameter and 5 mm in outer diameter. A direct current power source (BOHER HV, LAS-20 KV–50 mA, negative and positive polarity) is used to generate the atmospheric pressure discharge plasma in open air between a solid tungsten steel electrode (4 mm in diameter and with a hemisphere tip) and the flowing liquid surface. A graphite rod (5 mm in diameter) is placed at the bottom of the solution to act as an inert electrode. After plasma operation, we did not find an obviously visible change of the graphite electrode surface. The liquid acts as the cathode or anode, i.e. a positive or negative voltage applied to the tungsten steel electrode. After the plasma treatment, the treated liquid is mixed in a blending bottle by a magnetic stirrer. The liquid absorbance is detected in a flow cell, which is placed after the blending bottle (measured by Ocean Optics USB2000 + with a light source of DH-2000). The light source (DH-2000) continuously outputs from 200–2500 nm by using a combination of deuterium and tungsten halogen lamps. The flow cell (10 mm in optical length and 0.48 ml in volume) is made from JGS1 quartz with a suitable wavelength range of 200 nm–2500 nm. Because the liquid temperature can affect the absorbance intensity and peaks, we control it within a small deviation by a water cooling system to keep the liquid temperature to be about 25 °C. The discharge time is set to be 30 min. A 50 kΩ resistor is connected in series with the tungsten steel electrode to avoid the plasma transfer from glow-like discharge to arc. The discharge current is achieved from dividing the voltage across a 10 Ω resistor, which is, in series, connected with the graphite electrode.

The pH value and the solution conductivity are measured, by a pH detector (Yesmylab SX620) and a conductivity detector (Yesmylab SX650), respectively.

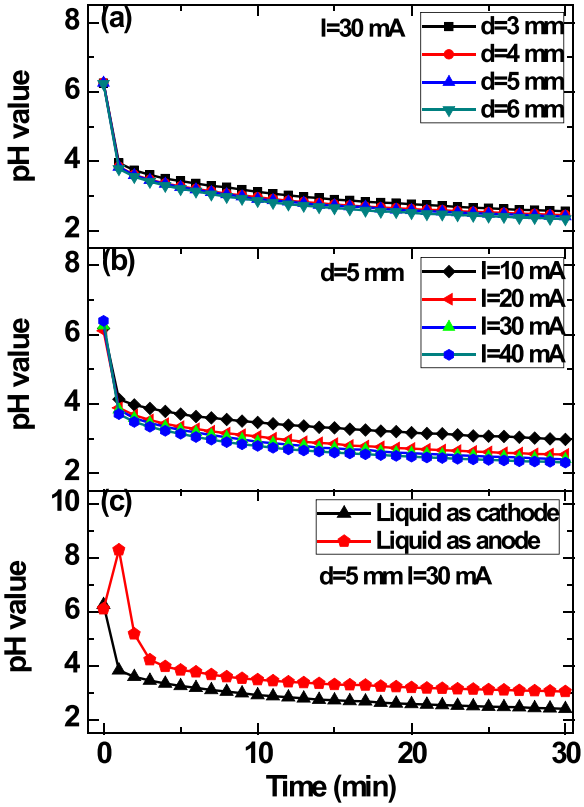

Figure 2. Solution pH value changes during the plasma treatment at (a) different discharge distances ($I = 30$ mA, liquid as cathode), (b) different discharge currents ($d = 5$ mm, liquid as cathode) and (c) liquid as cathode and as anode ($d = 5$ mm, $I = 30$ mA). The solution is an aqueous solution of sodium chloride with an initial conductivity of 3800 μS cm^{-1}.

The used reagents (analytical grade) of NaCl, $NaNO_2$ and $NaNO_2$ were purchased from Sinopharm Chemical Reagent Co., Ltd. Hydrogen peroxide (H_2O_2, 30%) was purchased from Xilong Scientific Co., Ltd.

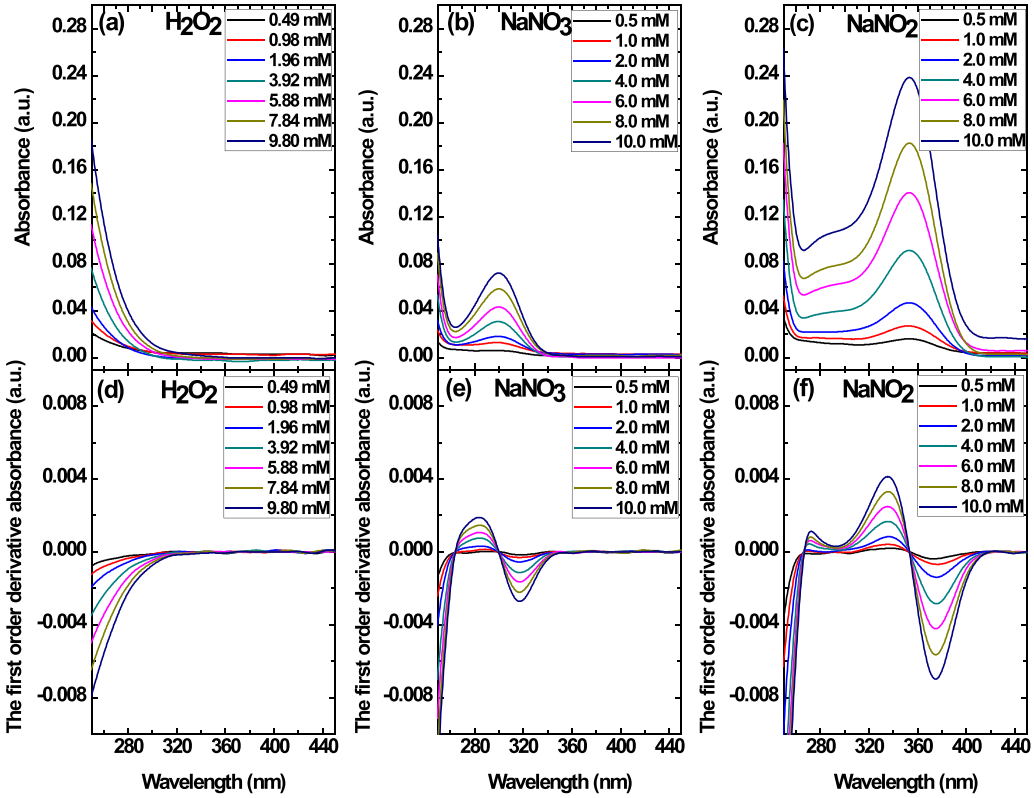

Figure 3. Absorbances and the first order derivative absorbances of the prepared standard stock solutions at different concentrations. (a), (d) for H_2O_2, (b), (e) for NO_3^- ($NaNO_3$), and (c), (f) for NO_2^- ($NaNO_2$).

Table 1. Real and measured concentrations of prepared standard stock solutions.

Prepared stock solutions		Real concentration (mM)	Measured concentration (mM)	Ratio of measured to the real concentration (%)
Stock solution 1 (pH value = 6.21)	H_2O_2	1.96	2.40 ± 0.04	122.45
	NO_3^-	3.00	3.15 ± 0.05	105.00
	NO_2^-	5.00	4.98 ± 0.02	99.60
Stock solution 2 (pH value = 6.18)	H_2O_2	2.94	3.26 ± 0.03	110.88
	NO_3^-	5.00	4.97 ± 0.04	99.40
	NO_2^-	2.00	1.94 ± 0.02	97.00
Stock solution 3 (pH value = 6.23)	H_2O_2	4.90	5.28 ± 0.05	107.76
	NO_3^-	2.00	2.10 ± 0.06	105.00
	NO_2^-	3.00	3.00 ± 0.02	100.00
Stock solution 4 (pH value = 6.19)	H_2O_2	2.94	3.26 ± 0.05	110.88
	NO_3^-	3.50	3.56 ± 0.06	101.71
	NO_2^-	3.50	3.48 ± 0.02	99.43

3. Results and discussion

Because the discharge plasma is operated in open air, nitrogen and oxygen gases are unavoidably involved in the discharge processes. As a result, nitrogen related oxides, N_xO_y, are formed in the gaseous plasma. When these N_xO_y transport towards the liquid phase, HNO_3 and HNO_2 are formed by a series of secondary processes, and that is the main reason for the solution acidification during an air plasma exposure. Hydroxyl (OH) radicals are produced mainly by the plasma-induced water decomposition. The combination of OH radicals leads to the formation of H_2O_2 in gaseous plasma and bulk liquid.

The generation of reactive species by the plasma–liquid interactions strongly depends on the voltage polarity applied to the system. We have confirmed that when the liquid acts as a cathode (a positive voltage is applied to the top tungsten steel electrode), the species generation rate is much faster than that in a liquid anode (a negative voltage is applied to the top tungsten steel electrode) because of the existence of a cathode voltage fall on the liquid surface [22]. Because the voltage fall is mainly varied with the solution conductivity, in order to sustain a stable cathode voltage fall, we must choose a solution with a suitable initial conductivity. Based on the results in [22], unless described otherwise, an aqueous

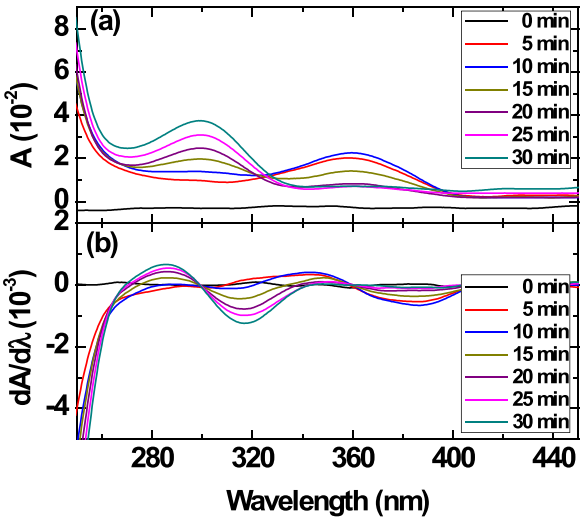

Figure 4. Absorbances (a) and the first order derivative absorbances (b) of the solution taken each 5 min during the air plasma treatment. The solution is an aqueous solution of sodium chloride with an initial conductivity of 3800 μS cm^{-1}. The solution acts as the cathode, the discharge distance is 5 mm and the discharge current is 30 mA.

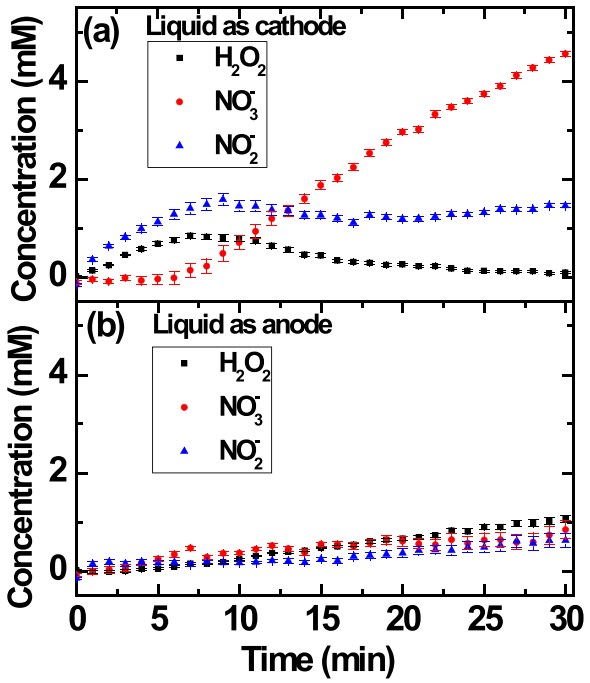

Figure 5. Temporal concentrations of generated H_2O_2, NO_3^- and NO_2^- for the liquid as (a) cathode and (b) anode during the plasma treatment. The solution is an aqueous solution of sodium chloride with initial conductivity of 3800 μS cm^{-1}. The discharge distance is 5 mm and the discharge current is 30 mA.

solution of sodium chloride with a conductivity of 3800 μS cm^{-1} is taken as the treated liquid in order to sustain relatively stable plasma–liquid interactions, since the cathode voltage fall keeps almost constant during the 30 min plasma treatment at this condition.

The pH value is an important parameter for the liquid chemistry, and therefore, we investigate the pH changes of plasma treated solutions at different conditions (figure 2). Obviously, solution acidification takes place in all cases. However, for the liquid anode case, there is a pH increase at first, and this can be explained as follows. In the liquid anode case, electrons, rather than ions, are driven to the liquid surface in the liquid cathode case, and therefore, OH^- is produced by equation (5) [42–44]. There exist two factors for the solution pH change at the same time, i.e. pH increases by the reaction of equation (5) and pH decreases by the above mentioned processes. At the beginning, the former is dominant, and after a certain time, the latter becomes dominant, leading to the pH behavior in the case of liquid anode.

$$2e^- + 2H_2O \rightarrow 2OH^- + H_2. \quad (5)$$

In our case, the first order derivative absorbance is used to achieve C_i. Figure 3 presents the absorbances and corresponding first order derivative absorbances of the prepared standard peroxide (H_2O_2), nitrate (NO_3^-) and nitrite (NO_2^-) at different concentrations. 44 $l\mathrm{d}\varepsilon_{i\lambda}/\mathrm{d}\lambda$ for each solution component are extracted from the data in figure 3(b) by linearly fitting the curve of $\mathrm{d}A_{i\lambda}/\mathrm{d}\lambda$ versus C_i based on the formula of $\mathrm{d}A_{i\lambda}/\mathrm{d}\lambda = l\mathrm{d}\varepsilon_{i\lambda}/\mathrm{d}\lambda C_i$. The selected 44 different wavelengths range from 260.86 nm to 380.58 nm (about each 2.8 nm), which covers the absorption contributions of H_2O_2, NO_3^- and NO_2^- (table A1). Using these standard $l\mathrm{d}\varepsilon_{i\lambda}/\mathrm{d}\lambda$ and the measured first order derivative absorbance of solutions, C_i can be obtained by performing multivariable linear regression to 44 equation (4)-like equations figure 3. Absorbances and the first order derivative absorbances of the prepared standard stock solutions at different concentrations. (a) and (d) for H_2O_2, (b) and (e) for NO_3^- ($NaNO_3$) and (c) and (f) for NO_2^- ($NaNO_2$).

In order to confirm the feasibility of our method, a series of standard stock solutions were prepared. Based on the $\mathrm{d}\varepsilon_{i\lambda}/\mathrm{d}\lambda$ in table A1, we calculated the concentrations of the mixed standard stock solutions, the measured concentrations for NO_3^- and NO_2^- are in good agreement with the real ones, while the calculated H_2O_2 concentrations show a relative difference from the real ones (table 1). These differences are considered to be the limited range of selected wavelengths which only includes a small part of the H_2O_2 absorption band, which has a peak band smaller than 260 nm. Actually, we have tried several wavelength ranges for determining the concentrations of three species in prepared standard stock solutions, and the best range is 260 nm to 380 nm. This might attribute to the considerable overlapping of absorbances among H_2O_2, NO_3^- and NO_2^- less than 260 nm. In spite of this problem, the change trend of the real H_2O_2 concentration can be represented by the estimated results if one checks table 1. That is to say, the NO_3^- and NO_2^- concentrations with a good accuracy, while the change trend of the H_2O_2 concentration can be estimated by this derivative absorption spectrophotometry in our experimental conditions.

Figure 4 presents the typical absorbance and the first order derivative absorbance of a plasma-treated NaCl solution. The absorbance shows a shoulder less than 280 nm, which is attributed to the H_2O_2, and the absorption bands at 300 nm and 350 nm are attributed to the species of NO_3^- and NO_2^-, respectively (see figure 3).

Each measurement is performed three times at the same condition. The measured values are averaged from these

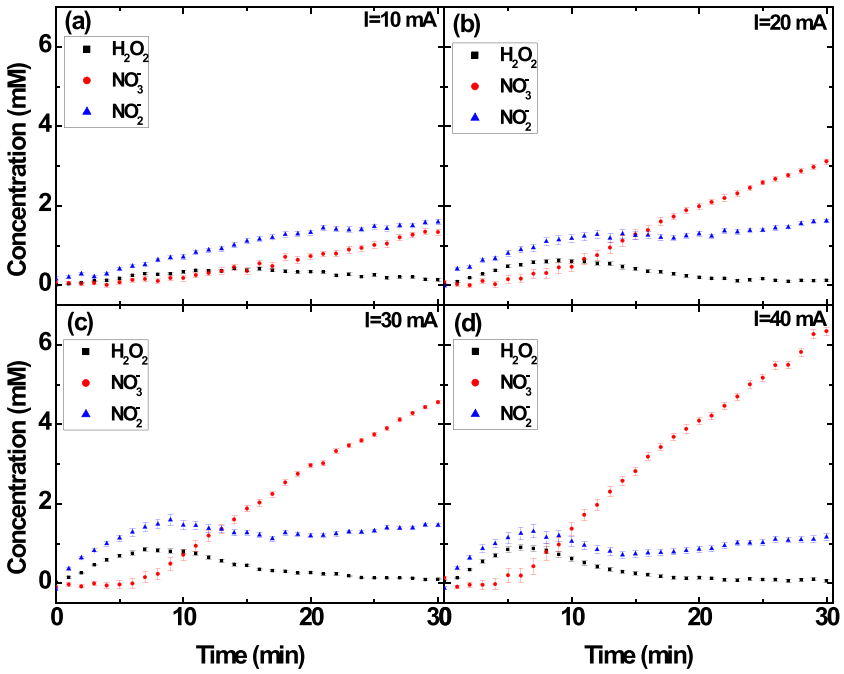

Figure 6. Temporal concentrations of generated H_2O_2, NO_3^- and NO_2^- for the aqueous solution of sodium chloride with an initial conductivity of 3800 μS cm^{-1} (liquid as cathode) at the discharge currents of (a) 10 mA, (b) 20 mA, (c) 30 mA and (d) 40 mA. The discharge time is 30 min and the discharge distance is 5 mm.

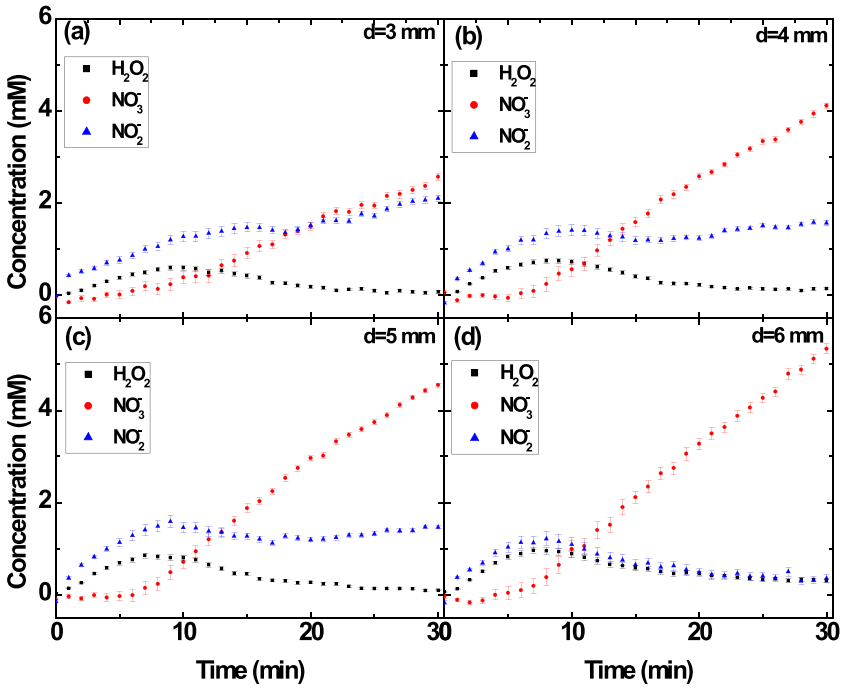

Figure 7. Temporal concentrations of generated H_2O_2, NO_3^- and NO_2^- for the aqueous solution of sodium chloride with an initial conductivity of 3800 μS cm^{-1} (liquid as cathode) at the discharge distances of (a) 3 mm, (b) 4 mm, (c) 5 mm and (d) 6 mm. The discharge time is 30 min and the discharge current is 30 mA.

results, and the error bars are the standard deviation of the measurements. Figure 5(a) presents the time evolutions of concentrations for H_2O_2, NO_3^- and NO_2^- which are calculated from the data in figure 4(b). The treated sodium chloride solution acts as the cathode. The discharge current and distance are 30 mA and 5 mm, respectively. The results are also shown in figure 5(b) for the experiment performed at the same condition except using a liquid anode.

For the case of liquid as the cathode, the concentrations of H_2O_2 and NO_2^- show a maximum point at about 8–9 min, while the concentration of NO_3^- is almost zero at the beginning of 7 min, and then increases until the end of the plasma treatment. It has been reported that peroxynitrous acid (ONOOH), an unstable isomer of HNO_3, can be formed through equation (6) when NO_2^- and H_2O_2 are present in a solution with a pH value of 3.3 [12],

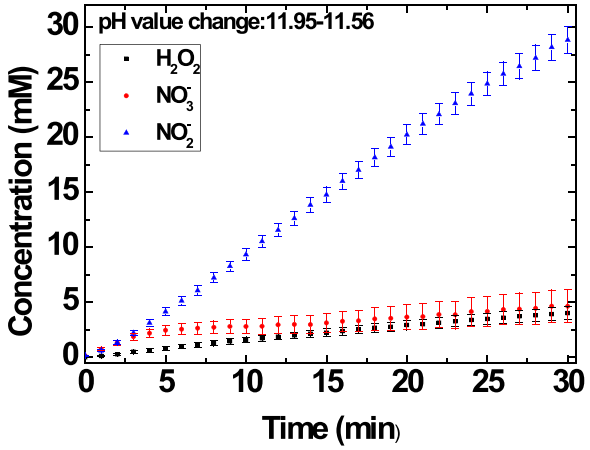

Figure 8. Temporal concentrations of generated H_2O_2, NO_3^- and NO_2^- for an aqueous solution of NaOH with initial conductivity of 3800 μS cm^{-1} during the plasma treatment (liquid as cathode). The discharge current and discharge distance are 30 mA and 5 mm, respectively.

$$H_2O_2 + NO_2^- + H^+ \rightarrow ONOOH + H_2O. \quad (6)$$

The peroxynitrous acid (with a pK_a of 6.8) dissociates slightly below neutrality, and it isomerises unimolecularly to HNO_3 with a rate constant of $k = 1.3\,s^{-1}$ at 25 °C, thus producing a final product of NO_3^- [45, 46]. If the pH value is much less than 7, the dissociation of peroxynitrous acid will be much faster. It is worth noting that in the dissociation of peroxynitrous acid, probably up to 5% of hydroxyl and nitrogen dioxide radicals are formed [47]. Figure 2 indicates that the critical pH value corresponding to the maximum concentration of NO_2^- and H_2O_2 is 3.0. On the other hand, most of NO_2^- (~71.5%) will exist in the form of molecular nitrous acid (HNO_2) at a pH value of 3.0, since the pK_a of nitrous acid is 3.4 [48]. It is known that the molecular nitrous acid is unstable and decomposes easily by disproportionation to nitrogen oxides via equation (7)

$$3HNO_2 \rightarrow H^+ + NO_3^- + 2NO + H_2O. \quad (7)$$

The above-mentioned first process consumes both H_2O_2 and NO_2^-, and the second one consumes NO_2^-. Consequently, the concentrations of H_2O_2 and NO_2^- decrease and that of NO_3^- increases during the plasma treatment. From figure 5(a), we can find that the production rate (the curve's slope) of NO_2^- is faster than that of H_2O_2 at the beginning, while the production rate of NO_3^- is almost zero. These results imply that in the case of liquid cathode, the primary aqueous species generated by plasma–liquid interactions are NO_2^- and H_2O_2 (the very first form being OH radicals and/or superoxide anion radicals or hydroperoxyl radicals depending on the pH value), and most of NO_3^- is a derivative species produced by reactions of NO_2^- and H_2O_2.

We also performed the experiments by varying the discharge current and discharge distance (figures 6 and 7). All of the data demonstrate similar results, which show support of our above explanation. The maximum concentrations of generated H_2O_2, and NO_2^- appears at a pH value of 3.0 (see figure 2).

In the case of liquid as anode, due to the lack of cathode voltage fall on the liquid surface, there is just low energy electron irradiation on the liquid surface [49], and the plasma–liquid interactions are much less intense than those in the liquid cathode case [22], causing considerably slow yields of species generated from the plasma–liquid interactions. The pH value of the liquid increases at first and then decreases (see figure 2(c)). The final pH value approaches 3.05, which is higher than the critical pH value (3.0 in our experimental conditions) for equation (6) to proceed. As a result, the concentrations of H_2O_2, NO_3^- and NO_2^- slowly increase during the whole plasma treatment.

In addition, although the NO_2^- in the form of molecular HNO_2 is easy to decompose, the ionic form of NO_2^- is considerably stable. Therefore, we treated an aqueous solution of NaOH by the air discharge plasma, and the pH value changes from 11.95 to 11.56 after the treatment (liquid as cathode). In this pH range, we consider that most of NO_2^- are in the ionic form, and they will not decompose or react with H_2O_2 (pH higher than the critical value) to form NO_3^-. This deduction is verified by the continuous increase of NO_2^- concentration as shown in figure 8.

4. Conclusions

We have presented a simple, fast derivative absorption spectroscopic method to *in situ* trace and quantify the aqueous H_2O_2, NO_3^-, and NO_2^- during the plasma–liquid interactions. Although there exist short-lived species during the plasma–liquid interactions, they either quench or react to form stable species, such as aqueous H_2O_2, NO_3^-, and NO_2^- finally. Therefore, in our experiment, we demonstrated that in the case of liquid cathode, the aqueous species in the plasma–liquid interactions are dominated by H_2O_2 and NO_2^-, and NO_3^- is produced by the reaction between H_2O_2 and NO_2^-, as well as by the dissociation of molecular HNO_2 at acidic condition. In the case of liquid anode, the concentrations of the aqueous H_2O_2, NO_3^- and NO_2^- increase slowly with the plasma treatment. This work realizes an *in situ*, direct, simultaneous probing of the evolution for H_2O_2, NO_3^- and NO_2^- during the plasma–liquid interactions. The applications of plasma–liquid interactions in water treatment and plasma medicine might benefit from the revelation of the pH value dependent processes during the plasma treatment.

Acknowledgments

The work was partially supported by National Natural Science Foundation of China (Grant Nos.: 11405144, 11304132, and 61376068), and the Fundamental Research Funds for the Central Universities (Grant Nos: 20720150022 and 20720150083). One of the authors XQ thanks the financial support from the Graduate Scientific Research and Innovation Foundation of Chongqing (No. CYS17007), and National '111' Project of China (Grant No: B08036).

Table A1. $l\mathrm{d}\varepsilon_i/\mathrm{d}\lambda$ data for peroxide (H_2O_2), nitrate (NO_3^-) and nitrite (NO_2^-).

Wavelength (nm)	$l\mathrm{d}\varepsilon/\mathrm{d}\lambda$ (mM^{-1})		
	H_2O_2	NO_3^-	NO_2^-
260.86	-5.29×10^{-4}	-1.63×10^{-4}	-4.83×10^{-4}
263.67	-4.74×10^{-4}	-1.99×10^{-5}	-2.13×10^{-4}
266.47	-4.21×10^{-4}	6.81×10^{-5}	1.69×10^{-5}
269.27	-3.72×10^{-4}	1.17×10^{-4}	8.98×10^{-5}
272.07	-3.26×10^{-4}	1.46×10^{-4}	1.23×10^{-4}
274.87	-2.83×10^{-4}	1.66×10^{-4}	1.16×10^{-4}
277.66	-2.44×10^{-4}	1.82×10^{-4}	9.50×10^{-5}
280.46	-2.10×10^{-4}	1.92×10^{-4}	7.69×10^{-5}
283.26	-1.81×10^{-4}	1.95×10^{-4}	6.24×10^{-5}
286.05	-1.55×10^{-4}	1.91×10^{-4}	4.95×10^{-5}
288.85	-1.32×10^{-4}	1.78×10^{-4}	3.94×10^{-5}
291.64	-1.12×10^{-4}	1.52×10^{-4}	3.39×10^{-5}
294.43	-9.49×10^{-5}	1.14×10^{-4}	3.37×10^{-5}
297.23	-8.04×10^{-5}	6.27×10^{-5}	3.87×10^{-5}
300.02	-6.74×10^{-5}	2.27×10^{-6}	4.89×10^{-5}
302.81	-5.58×10^{-5}	-6.30×10^{-5}	6.51×10^{-5}
305.60	-4.69×10^{-5}	-1.28×10^{-4}	8.46×10^{-5}
308.38	-3.87×10^{-5}	-1.84×10^{-4}	1.08×10^{-4}
311.17	-3.17×10^{-5}	-2.30×10^{-4}	1.37×10^{-4}
313.96	-2.56×10^{-5}	-2.59×10^{-4}	1.71×10^{-4}
316.74	-2.05×10^{-5}	-2.70×10^{-4}	2.07×10^{-4}
319.53	-1.78×10^{-5}	-2.64×10^{-4}	2.47×10^{-4}
322.31	-1.58×10^{-5}	-2.42×10^{-4}	2.88×10^{-4}
325.10	-1.45×10^{-5}	-2.12×10^{-4}	3.29×10^{-4}
327.88	-1.33×10^{-5}	-1.74×10^{-4}	3.65×10^{-4}
330.66	-1.27×10^{-5}	-1.37×10^{-4}	3.93×10^{-4}
333.44	-1.15×10^{-5}	-1.03×10^{-4}	4.10×10^{-4}
336.22	-9.40×10^{-6}	-7.47×10^{-5}	4.13×10^{-4}
339.00	-6.47×10^{-6}	-5.18×10^{-5}	3.98×10^{-4}
341.78	-5.58×10^{-6}	-3.34×10^{-5}	3.64×10^{-4}
344.56	-4.45×10^{-6}	-1.80×10^{-5}	3.08×10^{-4}
347.33	-3.96×10^{-6}	-8.71×10^{-6}	2.29×10^{-4}
350.11	-4.36×10^{-6}	-2.78×10^{-6}	1.31×10^{-4}
352.88	-5.83×10^{-6}	-1.03×10^{-6}	1.52×10^{-5}
355.66	-6.23×10^{-6}	-9.55×10^{-7}	-1.11×10^{-4}
358.43	-5.41×10^{-6}	-3.46×10^{-6}	-2.41×10^{-4}
361.20	-2.33×10^{-6}	-4.85×10^{-6}	-3.67×10^{-4}
363.97	-9.44×10^{-7}	-2.48×10^{-6}	-4.82×10^{-4}
366.74	6.70×10^{-7}	2.95×10^{-7}	-5.79×10^{-4}
369.51	1.63×10^{-6}	9.48×10^{-7}	-6.49×10^{-4}
372.28	2.03×10^{-6}	5.29×10^{-7}	-6.90×10^{-4}
375.05	1.68×10^{-6}	-6.00×10^{-8}	-7.00×10^{-4}
377.82	1.33×10^{-6}	-5.92×10^{-7}	-6.83×10^{-4}
380.58	1.54×10^{-6}	-1.92×10^{-6}	-6.41×10^{-4}

Appendix

Figure A1 shows the schematic diagram of the plasma–liquid interaction reactor. The cylinder-like cell is made from polytetrafluoroethylene and its geometric parameters are indicated in figure A1.

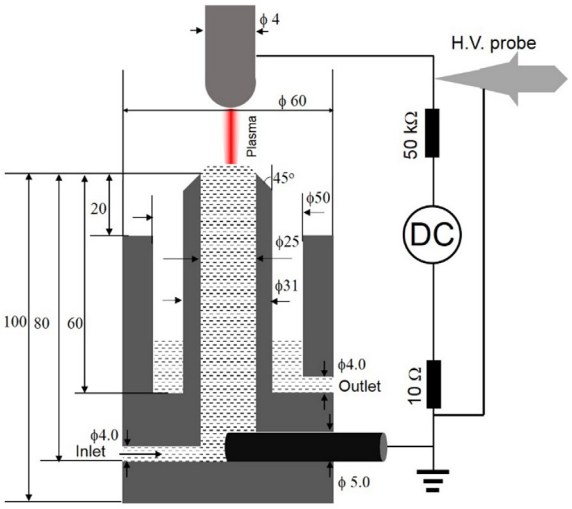

Figure A1. Schematic diagram of the plasma reactor.

ORCID iDs

Qiang Chen https://orcid.org/0000-0002-8688-1085

References

[1] Bruggeman P, Kushner M J, Locke B R, Gardeniers J, Graham W, Graves D B, Hofman-Caris R, Maric D, Reid J P and Ceriani E 2016 *Plasma Sources Sci. Technol.* **25** 053002
[2] Jamroz P, Gręda K, Pohl P and Żyrnicki W 2014 *Plasma Chem. Plasma Proc.* **34**
[3] Locke B, Sato M, Sunka P, Hoffmann M and Chang J-S 2006 *Ind. Eng. Chem. Res.* **45** 882
[4] Lukes P 2001 *Water Treatment by Pulsed Streamer Corona Discharge* (Prague: Institute of Plasma Physics AS CR)
[5] Fridman G, Friedman G, Gutsol A, Shekhter A B, Vasilets V N and Fridman A 2008 *Plasma Process. Polym.* **5** 503
[6] Kong M G, Kroesen G, Morfill G, Nosenko T, Shimizu T, Van Dijk J and Zimmermann J 2009 *New J. Phys.* **11** 115012
[7] Locke B R and Shih K-Y 2011 *Plasma Sources Sci. Technol.* **20** 034006
[8] Burlica R and Locke B R 2008 *IEEE Trans. Ind. Appl.* **44** 482
[9] Bobkova E, Shikova T, Grinevich V and Rybkin V 2012 *High Energy Chem.* **46** 56
[10] De Baerdemaeker F, Šimek M, Člupek M, Lukeš P and Leys C 2006 *Czech. J. Phys.* **56** B1132
[11] Lukes P, Appleton A T and Locke B R 2004 *IEEE Trans. Ind. Appl.* **40** 60
[12] Lukes P, Dolezalova E, Sisrova I and Clupek M 2014 *Plasma Sources Sci. Technol.* **23** 015019
[13] Hsieh K C, Wang H and Locke B R 2016 *Plasma Process. Polym.* **13** 908

[14] Thagard S M, Takashima K and Mizuno A 2009 *Plasma Chem. Plasma Process.* **29** 455
[15] Winter J, Tresp H, Hammer M, Iseni S, Kupsch S, Schmidt-Bleker A, Wende K, Dünnbier M, Masur K and Weltmann K 2014 *J. Phys. D: Appl. Phys.* **47** 285401
[16] Chen Q, Li J, Saito K and Shirai H 2008 *J. Phys. D: Appl. Phys.* **41** 175212
[17] Bruggeman P and Leys C 2009 *J. Phys. D: Appl. Phys.* **42** 053001
[18] Alshammari Y and Hellgardt K 2015 *Chem. Eng. Res. Des.* **93** 565
[19] Satterfield C N and Bonnell A H 1955 *Anal. Chem.* **2V7** 1174
[20] Dai X J, Corr C S, Ponraj S B, Maniruzzaman M, Ambujakshan A T, Chen Z, Kviz L, Lovett R, Rajmohan G D and de Celis D R 2015 *Plasma Process. Polym.* **13** 306
[21] Eisenberg G 1943 *Ind. Eng. Chem.* **15** 327
[22] Liu J, He B, Chen Q, Li J, Xiong Q, Yue G, Zhang X, Yang S, Liu H and Liu Q H 2016 *Sci. Rep.* **6** 38454
[23] Oliveira M C, Nogueira R F P, Neto J A G, Jardim W F and Rohwedder J J 2001 *Quim. Nova* **24** 188
[24] Sandell E B 1959 *Colorimetric Determination of Traces of Metals* (New York: Interscience)
[25] Nogueira R F P, Oliveira M C and Paterlini W C 2005 *Talanta* **66** 86
[26] Vasko C, Liu D-X, Van Veldhuizen E, Iza F and Bruggeman P 2014 *Plasma Chem. Plasma Process.* **34** 1081
[27] Miranda K M, Espey M G and Wink D A 2001 *Nitric Oxide* **5** 62
[28] Chen Q and Shirai H 2012 *Eur. Phys. J.* D **66** 1
[29] Feelisch M and Stamler J 1996 *Methods in Nitric Oxide Research* (New York: Wiley)
[30] Griess P 1879 *Eur. J. Inorg. Chem.* **12** 426
[31] Kitamura K and Majima R 1983 *Anal. Chem.* **55** 54
[32] Kus S, Marczenko Z and Obarski N 1996 *Chem. Anal.* **41** 899
[33] Peralta E, Roa G, Hernandez-Servin J, Romero R, Balderas P and Natividad R 2014 *Electrochim. Acta* **129** 137
[34] Oh J-S, Szili E J, Gaur N, Hong S-H, Furuta H, Short R D and Hatta A 2015 *J. Photopolym. Sci. Technol.* **28** 439
[35] Oh J-S, Szili E J, Gaur N, Hong S-H, Furuta H, Kurita H, Mizuno A, Hatta A and Short R D 2016 *J. Phys. D: Appl. Phys.* **49** 304005
[36] Szili E J, Oh J-S, Hong S-H, Hatta A and Short R D 2015 *J. Phys. D: Appl. Phys.* **48** 202001
[37] Owen T 2000 *Fundamentals of Modern UV–Visible Spectroscopy* (Waldbronn: Agilent Technologies)
[38] Suzuki N and Kuroda R 1987 *Analyst* **112** 1077
[39] Haaland D M, Easterling R G and Vopicka D A 1985 *Appl. Spectrosc.* **39** 73
[40] Kisner H J, Brown C W and Kavarnos G J 1983 *Anal. Chem.* **55** 1703
[41] Maris M A, Brown C W and Lavery D S 1983 *Anal. Chem.* **55** 1694
[42] Rumbach P, Witzke M, Sankaran R M and Go D B 2013 *J. Am. Chem. Soc.* **135** 16264
[43] Rumbach P, Bartels D M, Sankaran R M and Go D B 2015 *Nat. Commun.* **6** 8248
[44] Rumbach P, Bartels D M, Sankaran R M and Go D B 2015 *J. Phys. D: Appl. Phys.* **48** 424001
[45] Koppenol W, Moreno J, Pryor W A, Ischiropoulos H and Beckman J 1992 *Chem. Res. Toxicol.* **5** 834
[46] Oehmigen K, Winter J, Hähnel M, Wilke C, Brandenburg R, Weltmann K D and von Woedtke T 2011 *Plasma Process. Polym.* **8** 904
[47] https://en.wikipedia.org/wiki/Peroxynitrous_acid
[48] Stuehr D J and Nathan C 1989 *J. Exp. Med.* **169** 1543
[49] Shirai N, Uchida S and Tochikubo F 2014 *Japan. J. Appl. Phys.* **53** 046202